COMMUNICATIONS CHEMISTRY

ARTICLE

https://doi.org/10.1038/s42004-020-00390-1 OPEN

Understanding the interactions between the bis(trifluoromethylsulfonyl)imide anion and absorbed CO_2 using X-ray diffraction analysis of a soft crystal surrogate

Xin Zheng[1], Katsuo Fukuhara[1], Yuh Hijikata[2], Jenny Pirillo[2], Hiroyasu Sato[3], Kiyonori Takahashi[1,4], Shin-ichiro Noro[1,5,6]✉ & Takayoshi Nakamura[1,4,6]✉

The selective carbon dioxide (CO_2) absorption properties of ionic liquids (ILs) are highly pertinent to the development of methods to capture CO_2. Although it has been reported that fluorinated components give ILs enhanced CO_2 solubilities, it has been challenging to gain a deep understanding of the interactions occurring between ILs and CO_2. In this investigation, we have utilized the soft crystalline material $[Cu(NTf_2)_2(bpp)_2]$ (NTf_2^- = bis(trifluoromethylsulfonyl)imide, bpp = 1,3-bis-(4-pyridyl)propane) as a surrogate for single-crystal X-ray diffraction analysis to visualize interactions occurring between CO_2 and NTf_2^-, the fluorinated IL component that is responsible for high CO_2 solubility. Analysis of the structure of a CO_2-loaded crystal reveals that CO_2 interacts with both fluorine and oxygen atoms of NTf_2^- anions in a *trans* rather than *cis* conformation about the S–N bond. Theoretical analysis of the structure of the CO_2-loaded crystal indicates that dispersion and electrostatic interactions exist between CO_2 and the framework. The overall results provide important insight into understanding and improving the CO_2 absorption properties of ILs.

[1] Graduate School of Environmental Science, Hokkaido University, Sapporo 060-0810, Japan. [2] Institute for Chemical Reaction Design and Discovery (WPI-ICReDD), Hokkaido University, Sapporo 001-0021, Japan. [3] Rigaku Corporation, Akishima, Tokyo 196-8666, Japan. [4] Research Institute for Electronic Science, Hokkaido University, Sapporo 010-0020, Japan. [5] Faculty of Environmental Earth Science, Hokkaido University, Sapporo 060-0810, Japan. [6] These authors contributed equally: Shin-ichiro Noro, Takayoshi Nakamura. ✉email: noro@ees.hokudai.ac.jp; tnaka@es.hokudai.ac.jp

Ionic liquids (ILs) have received increasing attention in the past several decades owing to their wide variety of potential industrial applications[1–3]. This is especially true for ILs that have selective carbon dioxide (CO_2) absorption properties as a result of the tremendous interest in and urgency for stemming global warming by removal of green house gases from the atmosphere[4]. It is known that anion components of ILs significantly influence CO_2 absorption capacities and that fluorine containing anions are superior CO_2 absorbers as compared to those that lack this halogen[5]. This phenomenon is exemplified by the bis(trifluoromethylsulfonyl)imide (NTf_2^-) anion, which is one of the most interesting building blocks for the construction of ILs with high CO_2 absorption propensities[6]. Although several theories have been advanced to explain the physical interactions that take place between NTf_2^--containing ILs and CO_2, some of which have been tested experimentally and by using simulations[7–12], a full understanding of the interactions has not yet been gained. In particular, based on the current state of knowledge, it is still not possible to ascertain whether oxygen or fluorine is the key CO_2 absorption site in NTf_2^-, and to determine the nature of primary interactions occurring between this anion and this gas. The main hurdle to obtaining this information is associated with difficulties with determining the structures of ILs owing to their non-crystalline nature. In addition, the conformationally flexible structure of the NTf_2^- anion, originating from reasonably rapid rotation (barrier of 25.1 kJ mol^{-1}) of the CF_3SO_2 substituent around the S–N bond (Supplementary Fig. 13), complicates elucidation of the IL-CO_2 interactions.

Recently, a new class of materials, referred to as soft crystals, has attracted great attention. These materials can exist in both a highly crystalline and soft states, which can be reversibly interconverted in response to external chemical and physical stimuli[13,14]. Interestingly, some of the soft materials retain their single crystalline nature upon being treated with external stimuli. We envisaged that it might be possible to design and fabricate soft crystals, which contain components that are the same as or similar to those present in ILs, and that might possess the ability to absorb CO_2 in synchrony with stimuli promoted structural changes. In this way, it would be possible to utilize these substances as surrogates to determine the structures of and elucidate important interactions in ILs containing absorbed CO_2 using standard single-crystal X-ray diffraction techniques.

To explore this proposal, we prepared a new soft crystal [Cu$(NTf_2)_2$(bpp)$_2$] (**1**), which is composed of an NTf_2^- anion and the flexible 1,3-bis(4-pyridyl)propane (bpp) ligand and Cu^{2+} (Fig. 1) that possess an alkyl chain and positively charged Cu^{2+} coordinated nitrogen centers that are typical of those present in a ILs (e.g., the alkylimidazolium and NTf_2^- containing IL in Fig. 1). In the effort described below, we demonstrated that the soft crystal **1** displays reversible absorption of CO_2 associated with a stimulus-induced structural transformation, while retaining its permanent single-crystalline nature. Moreover, by using standard single-crystal X-ray diffraction techniques, we elucidated the nature of interactions with the NTf_2^- anion that are responsible for CO_2 absorption.

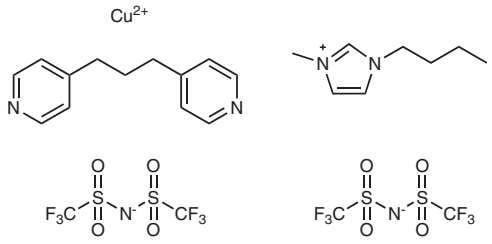

Fig. 1 Molecular structures. Structures of the components of soft crystal **1** (left) and a typical IL [1-*n*-butyl-3-methylimidazolium][NTf_2^-] containing NTf_2^- (right)[6].

Results

Crystal structure of as-synthesized soft crystal. A single-crystal of **1** was prepared by using the diffusion method and a three-phase system, including a 0.1 M aqueous Cu$(NTf_2)_2$ bottom layer, a 1:1 water and MeOH, middle layer, and 0.2 M bpp in MeOH top layer. Upon standing, this system generated transparent and rod-like purple single crystals, which were shown by using the elemental analysis to have the desired atomic composition and purity. The soft crystal **1** crystallized in the monoclinic space group *P*2/*n*, containing crystallographically independent one copper ion, two NTf_2^- anions and two bpp ligands. The copper ion, surrounded by two NTf_2^- anions and four bpp ligands, exists in a distorted octahedral environment (Fig. 2a). The distance between the copper ion and NTf_2^- anions (Cu1-O1 = 2.801(2) Å) is much longer than that between the copper ion and the bpp ligands (Cu1–N1 = 2.002(2) Å, Cu1–N2 = 2.013(3) Å) as a consequence of Jahn-Teller distortion and the weak coordination ability of NTf_2^-. The NTf_2^- anions exist in a *trans* conformation (Fig. 2b and Supplementary Fig. 1), which is known to be thermodynamically more stable than the *cis* conformation[15]. The bpp ligands bridge the copper ion to form one-dimensional (1D) chains oriented along the *b*-axis with a toroidal space of 6.4 Å × 12.2 Å (Fig. 2c and Supplementary Fig. 2). The 1D chains aggregate through weak CH/π interactions to form quasi two-dimensional (2D) layers with an interchain distance of 9.9 Å (Supplementary Fig. 3). In addition, NTf_2^- anions are sandwiched between the 2D layers through weak coordinative interactions, in which the distance between two neighboring layers is 8.0 Å (Supplementary Fig. 3). The 2D layers and NTf_2^- anions are densely packed through the above-mentioned weak coordinative interactions and weak hydrogen bonding interactions between the trifluoromethylsulfonyl groups of NTf_2^- and pyridyl groups of the bpp ligands (Supplementary Fig. 4). As a result, almost no pores exist in the crystal structure of **1**, and the pore space calculated by using MERCURY software (probe radius: 1.2 Å, approximately grid spacing: 0.7 Å) is only 0.7%.

CO_2 absorption properties and stability for water. Inspection of absorption/desorption isotherms of **1** displayed in Fig. 3a shows that almost no absorption of N_2 and Ar occurs at 77 K proving that this soft crystal has a densely assembled structure. In contrast, **1** exhibits a steep increase and decrease in the amount of absorbed CO_2 at $P/P_0 = 0.21$ and 0.09, respectively, and 195 K, while N_2 and Ar are not absorbed even at 195 K (Supplementary Fig. 9), which suggests that absorption of this gas takes place in association with a change between a closed and an open structure[16]. The saturated absorption amount of CO_2 was found to be 2.03 mol mol^{-1} at $P/P_0 = 0.98$ ($P \cong$ fugacity = 0.99 bar), which corresponds to 1.02 mol per mol of NTf_2^-. This value is close to those of NTf_2^--containing CO_2 absorbing ILs at 313 K and 40 bar (fugacity = 34 bar) (under this condition, absorption by NTf_2^--containing ILs is ca. 0.5 CO_2 mole fraction, corresponding to 1 mol per one mol of NTf_2^-)[17]. In order to elucidate the role of fluorinated moieties in governing CO_2 absorption, we synthesized the nonfluorinated analog of [Cu$(NMes_2)_2$(bpp)$_2$] (**2**), in which $NMes_2^-$ is bis(methylsulfonyl)imide, which has a one-dimensional structure that is similar to that of **1** (Supplementary Fig. 6) and measured its absorption properties. As shown in Fig. 3a and Supplementary Fig. 10, CO_2 is selectively absorbed to **2** but the threshold pressure in the absorption isotherm (P/P_0 = 0.32) is higher than that of **1** ($P/P_0 = 0.21$), indicating that the

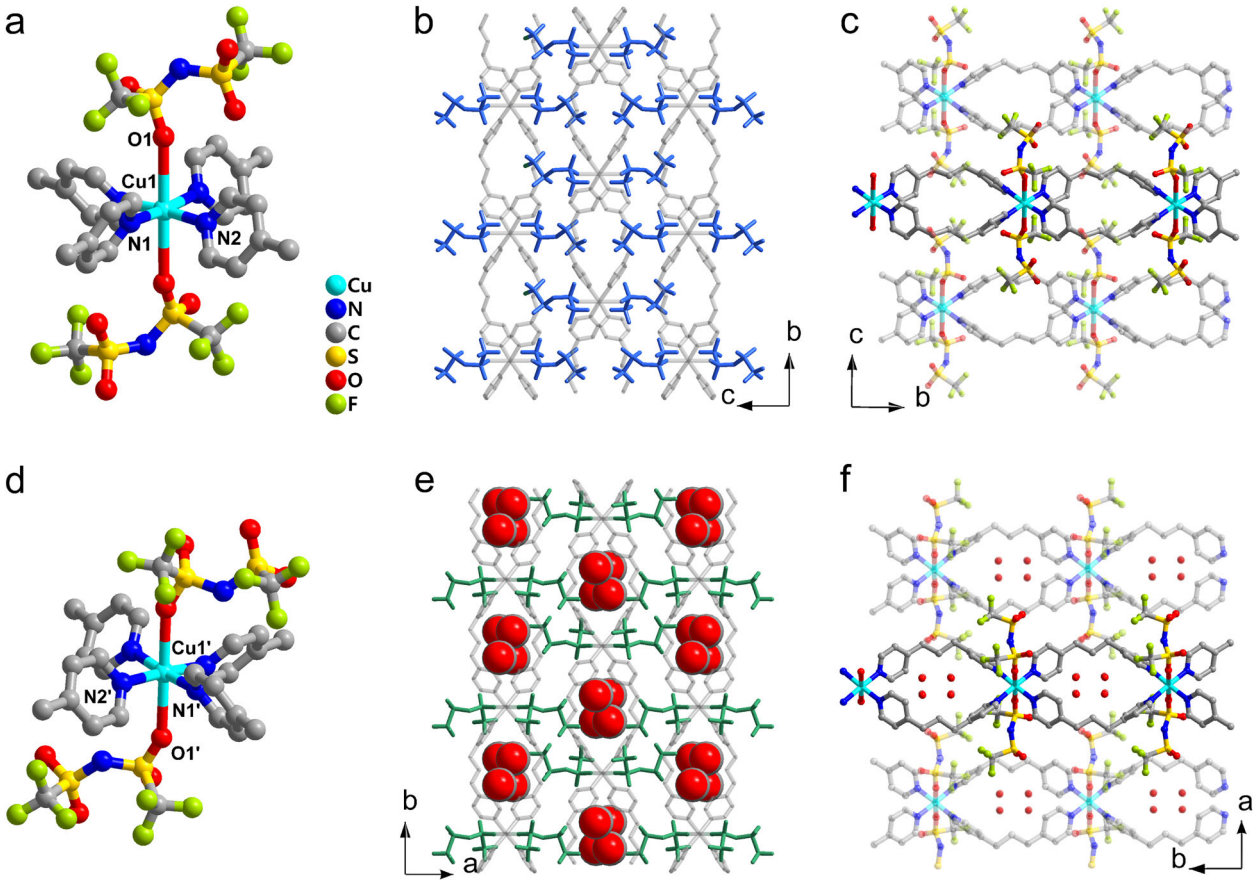

Fig. 2 Crystal structures. Views of the crystal structures of **a**–**c 1** and **d**–**f 1**·2CO_2. Coordination environment around the Cu center in **a 1** and **d 1**·2CO_2. Conformation of NTf_2^- in **b 1** and **e 1**·2CO_2. 1D chain structures in **c 1** and **f 1**·2CO_2.

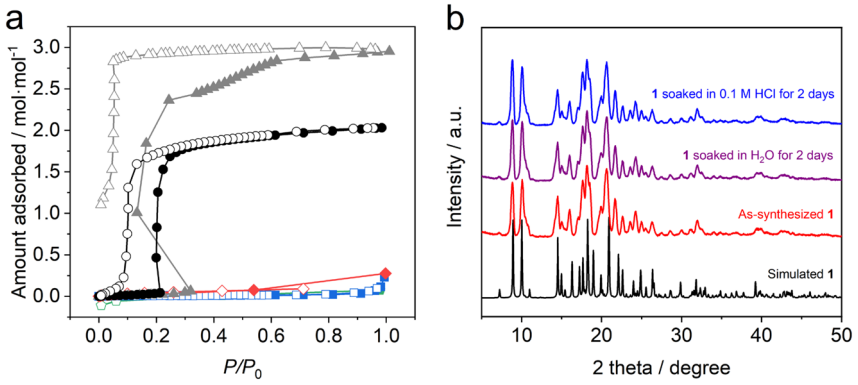

Fig. 3 Absorption/desorption properties and PXRD patterns. a Absorption (closed symbols)/desorption (open symbols) isotherms of CO_2 (black circle), N_2 (blue square), Ar (green pentagon), and H_2O (red rhombus) at 195 K (CO_2), 77 K (N_2 and Ar), and 298 K (H_2O), respectively, for **1** and of CO_2 (gray triangle) at 195 K for **2**. **b** Calculated PXRD pattern of **1** from its single-crystal X-ray structure (black) and observed PXRD patterns of as-synthesized **1** (red), **1** soaked in H_2O (purple) and 0.1 M HCl (blue) for 2 days.

fluorinated component facilitates the CO_2 absorption. A similar observation has been made in studies of the ILs with NTf_2^- and $NMes_2^-$ anions[5]. The integer number (2 mol mol^{-1}) of the amount of CO_2 absorbed at saturation may be related to the free volume and/or specific absorption sites in the soft crystal **1**.

The results of investigation of the variable-temperature CO_2 absorption of **1** reveal that similar behavior is followed but that different threshold pressures exist in the absorption and desorption isotherms (Supplementary Fig. 11). Because the threshold positions are related to equilibrium pressures for the CO_2 absorption reaction, their temperature dependence enables an evaluation of the enthalpy of CO_2 absorption (Q_{st}) by using the Clausius-Clapeyron equation. A plot of the natural logarithm of the threshold positions vs $1/T$ was found to be linear (Supplementary Fig. 12), and analysis of the slope yields a Q_{st} value of -29.1 kJ mol^{-1}. This enthalpy value is only moderate when compared with those of other CO_2 absorption/adsorption materials, including a 30 wt% monoethanolamine solution (-72 to -79 kJ mol^{-1})[18], amine-functionalized porous organic polymer (-61 kJ/mol)[19] and zeolites (-49.1, -50.0, and −38.0 kJ mol^{-1} for NaX, Na-ZSM-5 and H-ZSM-5, respectively)[20]. [1-*n*-Alkyl-3-methylimidazolium][NTf_2^-] (alkyl = ethyl, butyl, and hexyl) ILs

have smaller Q_{st} values ranging from -11 to -14 kJ mol^{-1} because of more limited physisorption between dynamic liquid and a gas phase[21]. The only moderate Q_{st} value among those of other solid adsorbents suggests that the interaction between NTf_2^- in **1** and CO_2 and/or that between bpp and CO_2 is not strong.

The stability and absorbability of **1** for water, which are important issues when contemplating practical uses, were also investigated. NTf_2^- anion is hydrophobic as reflected by the fact that the IL [1-*n*-butyl-3-methylimidazolium][NTf_2^-] (Fig. 1) has a low absorbability for water and a CO_2 absorption capacity that is not affected by water absorption[17]. The soft crystal **1** also has negligible H_2O absorbability (Fig. 3a). Furthermore, soaking in neutral and acidic (0.1 M HCl) H_2O for 2 d does not affect the powder X-ray diffraction (PXRD) patterns of **1** (Fig. 3b). These results show that **1** has outstanding stability and low water absorbability.

Crystal structure of CO_2-loaded soft crystal. Because soft crystal **1** retains its single crystalline nature after absorption of CO_2, we were able to determine the structure of the CO_2-loaded crystal **1**·2CO_2 by using standard single-crystal X-ray diffraction analysis. The space group of **1**·2CO_2 was found to be *C*2/*c*, which can be considered as being a transform to a *C*-centered lattice with space group *P*2/*n*. The coordination environments of the copper ion in **1** and **1**·2CO_2 are similar (Figs. 2a and 2d), while the distance between the copper center and NTf_2^- anion is 7% shorter (Cu1′-O1′ = 2.600(2) Å) and that between the copper center and bpp ligands is slightly longer (Cu1′–N1′ = 2.015(3) Å, Cu1′–N2′ = 2.018(3) Å) in **1**·2CO_2 compared to **1**. The toroidal shape of 1D chains in **1**·2CO_2 are almost unchanged (6.3 Å × 12.3 Å, Fig. 2f and Supplementary Fig. 2) in comparison with **1**, and the dihedral angles of neighboring pyridine rings coordinated to the same copper ions decrease from 69°/68° in **1** to 59°/64° in **1**·2CO_2. Moreover, **1**·2CO_2 contains slightly different quasi 2D layers in comparison to **1**. Specifically, each 1D chain in **1**·2CO_2 is inclined against the plane composed of copper ions, resulting in a slightly larger interchain distance (10.3 Å) (Supplementary Fig. 3). The interlayer space is occupied by both NTf_2^- anions and CO_2 molecules, and the presence of absorbed CO_2 causes a significant expansion of the interlayer distance from 8.0 to 8.6 Å (Supplementary Fig. 3). Consequently, the cell volume of **1**·2CO_2 is 8.5 % larger than that of **1** largely because of a 7.5% expansion of the interlayer.

As mentioned above, all NTf_2^- anions in **1** are arranged in a parallel manner in the *trans* conformation. However, after CO_2 absorption, six NTf_2^- anions exist in a *cis* conformation (Supplementary Fig. 1) and are positioned at corners of hexagonal vertexes (Supplementary Fig. 5) to form a cavity which encloses two CO_2 molecules (Fig. 2e). The significant changes taking place in the interlayer distance and conformation of NTf_2^- anions, along with other slight structural changes suggest that the soft crystal **1** undergoes an induced-fit type change to accommodate CO_2.

Interactions that exists between the 1D chains and CO_2 in **1**·2CO_2 are shown in Fig. 4. CO_2 molecules in **1**·2CO_2 are disordered over two sites with occupancies of 0.66 (molecule A) and 0.34 (molecule B). The shortest contact exists between a fluorine of one NTf_2^- anion and the carbon of CO_2 with F•••C distances of 2.95(2) (molecule A) and 2.68(5) Å (molecule B), which are shorter than the sums of their van der Waals radii (3.05–3.23 Å)[22]. On the other hand, the distances between oxygen of another NTf_2^- anion and the carbon of CO_2 in molecule A (O•••C = 3.02(2) Å) and molecule B (O•••C = 3.28(5) Å) are comparable with the sums of their van der Waals radii (3.00–3.35 Å)[22]. Considering that molecule A has a larger occupancy, it is expected that both fluorine and oxygen in the NTf_2^- anion should play prominent roles in governing CO_2 absorption. Weak hydrogen bonding interactions also exist between the bpp ligand and CO_2 (H•••O and C•••O = 2.52(2) and 3.30(2) Å & 2.91(4) and 3.42(4) Å in molecule A and 2.58(4) and 3.34(4) Å & 2.83(6) and 3.34(6) Å in molecule B, Fig. 4).

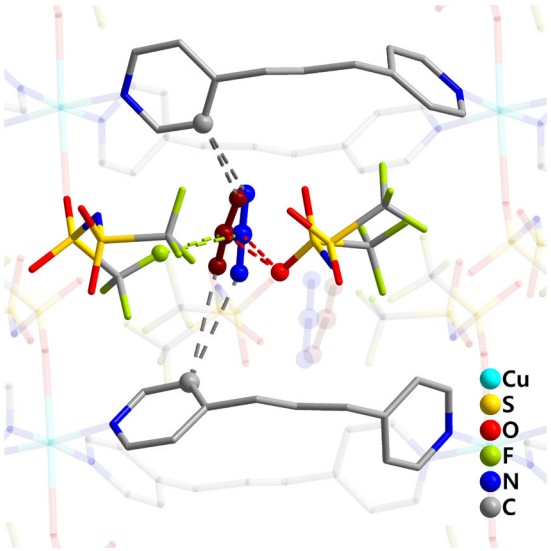

Fig. 4 CO_2-Absorbed structure. View of the intermolecular contacts between the CO_2 molecule (blue: molecule A, red: molecule B) and structural components in **1**·2CO_2.

The degree of quadrupole-quadrupole interactions between CO_2 molecules is related to the distances between the carbons of two neighboring CO_2 molecules. In **1**·2CO_2, the respective distances between CO_2 carbons in molecules A and A, molecules A and B, and molecules B and B are 3.82(3) Å, 4.03(6) Å and 4.28 (8) Å. Although the crystal structure of **1**·2CO_2 was determined at a temperature below the sublimation point of CO_2, the intermolecular C–C distances are longer than the intermolecular distance (3.58 Å) in solid CO_2[23]. Moreover, the C–C distance between CO_2 molecules in molecules B and B is greater than 4.1 Å, which is the intermolecular C–C distance in gaseous CO_2[24]. The differences in the intermolecular CO_2•••CO_2 distances show that a quadrupole-quadrupole interaction contributes little to stabilization of absorbed CO_2 in **1**·2CO_2 and, consequently, demonstrate that interactions with both a fluorine and oxygen atom in the NTf_2^- anion are the most influential in governing absorption of CO_2 gas by **1**.

Theoretical calculations. A density functional theory calculation was performed under periodic boundary conditions to gain more information about interactions occurring between NTf_2^- anions and CO_2 in **1**·2CO_2. The binding energy (E_b) was determined by using the equation $E_b = E_{Framework+gas} - (E_{Framework} + E_{Gas})$, where $E_{Framework+gas}$ and $E_{Framework}$ are the respective energies of the complete complex **1**·2CO_2 and only the framework of **1**·2CO_2, and E_{Gas} is the energy of CO_2 in a sufficiently large super cell. The calculated E_b value was found to be -31.3 kJ mol^{-1}, which is consistent with the experimentally determined enthalpy of CO_2 absorption. Next, an analysis of the interaction of **1**·2CO_2 was performed, utilizing a cluster model and an energy decomposition analysis with the natural orbitals from chemical valence theory, in order to elucidate the nature and trend of the interaction that most strongly contributes to CO_2 absorption. The results (Supplementary Table 4) show that large contributors to the stabilization of the structure of **1**·2CO_2 are a dispersion force (-28.7 kJ mol^{-1}) and an electrostatic interaction (-25.0 kJ mol^{-1}), and that

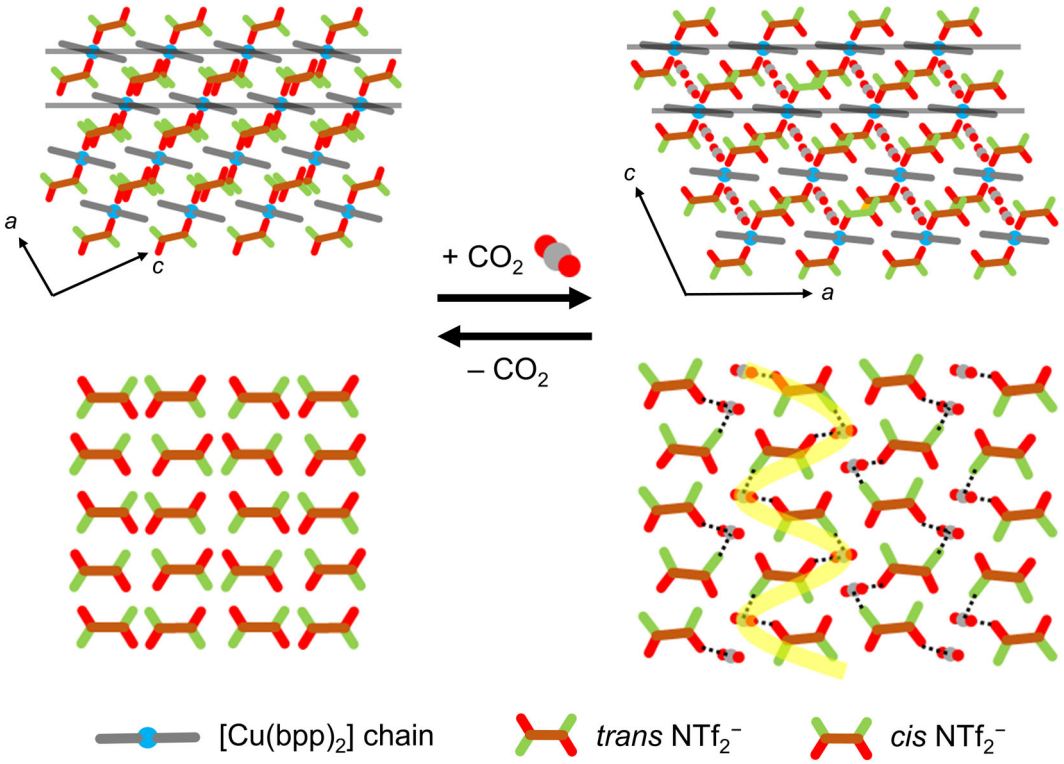

Fig. 5 Schematic representation of CO_2 absorption process. Schematic views of structural changes occurring in the CO_2 absorption process by soft crystal **1**. The upper figures show packing structures viewed along the *b*-axis and bottom figures show arrangements of NTf_2^- anions in the presence and absence of CO_2. The 1D [Cu(bpp)$_2$] chains are oriented along the *b*-axis. The dotted lines indicate intermolecular interactions between the NTf_2^- anion and CO_2. The yellow meandering line shows the 1D alternate arrangement of •••NTf_2^-•••CO_2•••NTf_2^-•••CO_2•••.

orbital interaction energy (−13.3 kJ mol^{-1}) is a minor contributor. This result is consistent with previous findings, which suggest that calculated Lewis acid-base binding energies between CO_2 and naked anions are inversely proportional to the solubility of CO_2 in ILs. Thus, Lewis acid-base interactions are not important contributors to solubilities of CO_2 in ILs[25].

Discussion

In Fig. 5 are displayed schematic views of the structures of soft crystal **1** formed during the CO_2 absorption process. Analysis of the structures before and after CO_2 absorption shows that the CO_2 absorption process by **1** has features that are similar to those of ILs. Firstly, **1** preferably absorbed CO_2 over other gases such as N_2 and Ar. Secondly, during absorption, the lattice of **1** expands to create an interstitial space for CO_2[26], while the distance between the cation (in this case, copper) and anion (in this case, NTf_2^-) changes only slightly[27]. In addition, our studies have uncovered a unique feature not observed previously in studies of CO_2 absorption by ILs. Specifically, we obtained direct evidence showing that the NTf_2^- anion undergoes a conformational change from the *trans* to *cis* upon CO_2 binding. In ILs, the NTf_2^- anion can exist in two possible conformations (*trans* and *cis*) at room temperature with the *trans* form being thermodynamically more stable[15,28]. The reason why the conformation of the NTf_2^- anion changes when **1** absorbs CO_2 is that cohesion energy is enhanced owing to the larger dipole moment of the *cis* form (dipole moments for *trans* and *cis* forms are 0.2–0.4 and 4.4–5.4, respectively)[29]. This enables the absorbed CO_2 molecule interact more strongly and cooperatively with the fluorine and oxygen atoms of the two neighboring *cis*- NTf_2^- anions by taking full advantage of delocalized negative charges (Supplementary Table 3), in the 1D alternate arrangement of •••NTf_2^-•••CO_2•••NTf_2^-•••CO_2•••.

Gas absorption taking place in association with a change between a closed structure and an open structure of an absorbent is dominated by a balance between the energy barrier for the structural transition of the absorbent and the enthalpy change associated with the open form absorbing the gas[30,31]. The fluorinated moieties contribute to decreasing the energy barrier for the structural transition because they have an ability to delocalize charge (Supplementary Table 3) and low electronic polarizability that leads to weakening intermolecular interactions[32]. The effect of the fluorinated groups on the gas absorption enthalpy change is likely not related to Lewis basicity because the result of this study reveal that Lewis acid-base interactions are not important contributors to solubilities of CO_2. Indeed, the most basic sites in anions are close to the most acidic sites in cations, which prevents the occurrence of Lewis acid-base interactions between CO_2 and the most basic sites. Although the issue requires more detailed studies, it appears that charge delocalization and low electric polarizability promoted by fluorination have respective impacts on electrostatic interactions and dispersion forces that influence CO_2 absorption.

Prior to the study described above, numerous experiments have been conducted to elucidate the CO_2 absorption states in ILs[7–12]. In this effort, using the soft crystal **1** as a surrogate, we were able to visualize interactions that occur between the NTf_2^- anion component of ILs and CO_2. The pyridine rings in bpp ligands and NTf_2^- anions in **1** synergistically constrain CO_2 molecules in the crystal. The NTf_2^- anion contains the primary absorption sites for CO_2 comprised of a trifluoromethyl fluorine and sulfonyl oxygen atom. The bpp ligand supports the NTf_2^--CO_2 interaction through the formation of a weak phenyl hydrogen-CO_2

interaction. As a result, a dispersion force and electrostatic interaction are the main contributors to stabilization of the CO_2-absorbed complex. Furthermore, a conformational change of the NTf_2^- anions from *trans* to *cis* occurring upon CO_2 capture by **1** also contributes to the absorption capacity. Of course, we understand that the observations made in this investigation have been made using a surrogate and not under real IL conditions especially because of differences in temperature and fluidity of the system. In addition, ILs with the NTf_2^- anion are not practical for CO_2 separation because the perfluorinated groups containing NTf_2^- anion is not an environment-friendly. Nevertheless, the findings should not only increase the level of understanding of CO_2 absorption by ILs but also provide new approaches to probe interactions between ILs and CO_2 and to design new systems for CO_2 separation applications.

Methods

Synthesis. Commercially available reagents were used as received without further purification. $Cu(NTf_2)_2$ and $Cu(NMes_2)_2$ were synthesized using previously described procedures[28,33].

A single-crystal of $[Cu(NTf_2)_2(bpp)_2]$ (**1**) was prepared by using a diffusion method in the straight glass tube containing a bottom layer of 0.1 M aqueous Cu $(NTf_2)_2$, a middle layer of 1:1 water and MeOH, and a top layer of 0.2 M bpp in MeOH. After 1 week, the formed transparent and rod like purple single crystals were separated by filtration, washed with water, and dried in the atmosphere. Elemental analysis was used to confirm the atomic composition and purity of the as-synthesized single crystals. Elemental analysis (%) calcd for $C_{30}H_{28}Cu_1F_{12}N_6O_8S_4$: C 35.31, H 2.77, N 8.24, F 22.34, S 12.57. Found: C 34.86, H 2.57, N 8.04, F 22.77, S 12.69. The thermogravimetric curve and Fourier transform infrared spectrum of **1** are shown in Supplementary Figs. 7 and 8.

A single-crystal of $\{[Cu(NMes_2)_2(bpp)_2]\cdot 3H_2O\}$ (**2**·$3H_2O$) was prepared by using a solvent evaporation method in the beaker containing 0.1 M aqueous Cu $(NMes_2)_2$ and 0.2 M bpp in MeOH. After 1 week, the formed transparent and plate like blue single crystals were separated by filtration, washed with MeOH, and dried in the atmosphere. This crystal lost a part of hydrated water during drying, which was confirmed using elemental analysis. Elemental analysis (%) calcd for $C_{30}H_{44.4}Cu_1N_6O_{10.2}S_4$ (**2**·$2.2H_2O$): C 42.69, H 5.30, N 9.96. Found: C 42.20, H 4.98, N 9.76. A single-crystal of $[Cu(NMes_2)_2(bpp)_2]$ (**2**) was prepared by drying **2**·$3H_2O$ under N_2 flow at 373 K for 30 min.

Single-crystal X-ray diffraction analysis of 1, 1·2CO$_2$, and 2. Crystal data for **1** were collected at 173 K on a RIGAKU RAXIS-RAPID imaging-plate diffractometer with a graphite-monochromated Mo-Kα radiation ($\lambda = 0.71075$ Å). Crystal data for **2** were collected at 293 K on a RIGAKU XtaLab Synergy-R with a multi-mirror monochromated Mo-Kα radiation ($\lambda = 0.71075$ Å). The structures were solved by using direct method (SHELXT)[34] and refined by using full-matrix least-squares techniques on F^2 using SHELXL-2018[35]. All non-hydrogen atoms were refined anisotropically. Hydrogen atoms were located at geometrically calculated positions and refined using a riding model. Olex2 was used as a graphical user interface[36]. Crystallographic data are shown in Supplementary Tables 1 and 2 and Supplementary Data 1 and 3.

The structural determination of **1**·$2CO_2$ was carried out using the following procedure. A single crystal of **1** was placed at the bottom of a glass capillary, which was then adhered to the base using glue. The base was installed on the absorption equipment (BELSORP-mini, MicrotracBEL Corp.) and the crystal was heated at 373 K for 30 min under a vacuum as the pre-treatment. After pre-treatment, CO_2 gas at 40 kPa was added and the capillary was cut and sealed quickly. The capillary containing single crystal sample and CO_2 gas was placed in the single-crystal X-ray diffractometer with a cryogenic unit, and cooled at a rate of 1 K min^{-1} from 293 K to 173 K, and then held at 173 K for 4 h. X-ray diffraction measurements were then made at 173 K on a RIGAKU XtaLAB P200 with a multi-mirror monochromated Cu-Kα radiation ($\lambda = 1.5418$ Å). Data analysis was performed in the manner described for **1**. Crystallographic data are shown in Supplementary Table 1 and Supplementary Data 2.

Gas absorption isotherm experiments. CO_2 (195 K), N_2 (77 K and 195 K) and Ar (77 K and 195 K) absorption/desorption isotherms were measured by using a BELSORP-max (MicrotracBEL Corp.). Water absorption/desorption isotherms were measured at 298 K by using a BELSORP-aqua (MicrotracBEL Corp.). Before the measurement, the sample was heated at 373 K in a vacuum overnight for activation by BELPREP-vac (MicrotracBEL Corp.). High-pressure CO_2 absorption/desorption isotherms were measured by using a BELSORP-HP (MicrotracBEL Corp.). Activation of the sample was performed on a BELSORP-HP at 373 K in a vacuum.

Theoretical calculations. For determining the S–N bond rotational barrier in NTf_2^-, relax scan calculations were performed using gaussian 09 Rev. E.01 software at the B3LYP/aug-cc-pVDZ level of theory[37]. A PBE functional[38], with projector augmented wave potentials and van der Waals interaction corrected by using a D3 scheme[39] to optimize the atomic positions of **1**, CO_2 and **1**·$2CO_2$, was used to obtain an estimate of the binding energy of CO_2 (Supplementary Fig. 14). In all cases, spin polarized calculations were employed under periodic boundary condition and Γ-point approximation using the Vienna Ab initio Simulation Package (VASP)[40–43] with the cut-off energy of 400 eV. The atomic charges were evaluated based on Bader analysis (Supplementary Table 3)[44–47]. In a manner that is similar to other reported approaches[48–50], after optimization of **1**·$2CO_2$, a model consisting of one CO_2, three NTf_2^- and three (4-pyridyl)butane, which are protonated instead of bonded to Cu^{2+} (Supplementary Fig. 15), was employed to investigate the nature of the interaction between CO_2 and **1**. The positions of added H atoms were optimized with a PBE functional using Amsterdam Density Functional 2018 program[51]. A standard triple-ζ STO basis set with two sets of polarization functions (TZ2P)[52] and a Grimme D3 type dispersion correction were applied to all atoms in the model. The model structure was optimized and analyzed by using the energy decomposition method[53] combined with the natural orbitals for chemical valence theory[54,55] with the same level of theory as that used for optimization of H atoms.

Data availability

Crystallographic data for the structures reported in this manuscript have been deposited at the Cambridge crystallographic Data Centre under deposition numbers CCDC 1981481 (**1**, Supplementary Data 1), 1981483 (**1**·$2CO_2$, Supplementary Data 2), and 2021731 (**2**, Supplementary Data 3). Copies of the data can be obtained free of charge via https://www.ccdc.cam.ac.uk/structures/. All other relevant data that support the findings of this study are available within the manuscript and its Supplementary Information, or from the corresponding author upon reasonable request.

Received: 13 February 2020; Accepted: 29 September 2020;
Published online: 27 October 2020

References

1. Seddon, K. R. Ionic liquids for clean technology. *J. Chem. Technol. Biotechnol.* **68**, 351–356 (1997).
2. Zhao, D. et al. Ionic liquids: applications in catalysis. *Catal. Today* **74**, 157–189 (2002).
3. Plechkova, N. V. & Seddon, K. R. Applications of ionic liquids in the chemical industry. *Chem. Soc. Rev.* **37**, 123–150 (2008).
4. Lei, Z. et al. Gas solubility in ionic liquids. *Chem. Rev.* **114**, 1289–1326 (2014).
5. Pringle, J. M. et al. The effect of anion fluorination in ionic liquids-physical properties of a range of bis(methanesulfonyl)amide salts. *N. J. Chem.* **27**, 1504–1510 (2003).
6. Anthony, J. L. et al. Anion effects on gas solubility in ionic liquids. *J. Phys. Chem. B* **109**, 6366–6374 (2005).
7. Kelley, S. P. et al. Understanding carbon dioxide solubility in ionic liquids by exploring the link with liquid clathrate formation. *Chem. Eur. J.* **23**, 14332–14337 (2017).
8. Rao, S. S. & Gejji, S. P. CO_2 Absorption using fluorine functionalized ionic liquids: interplay of hydrogen and σ-hole interactions. *J. Phys. Chem. A* **120**, 1243–1260 (2016).
9. Damas, G. B. et al. A quantum chemistry study for ionic liquids applied to gas capture and separation. *J. Phys. Chem. B* **118**, 9046–9064 (2014).
10. Ramdin, M. et al. State-of-the-Art of CO_2 Capture with Ionic Liquids. *Ind. Eng. Chem. Res.* **51**, 8149–8177 (2012).
11. Hu, Y. F. et al. The molecular characteristics dominating the solubility of gases in ionic liquids. *Chem. Soc. Rev.* **40**, 3802–3823 (2011).
12. Lourenço, T. C. et al. Insights on the solubility of CO_2 in 1-ethyl-3-methylimidazolium bis(trifluoromethylsulfonyl)imide from the microscopic point of view. *Environ. Sci. Technol.* **47**, 7421–7429 (2013).
13. Horike, S. et al. Soft porous crystals. *Nat. Chem.* **1**, 695–704 (2009).
14. Kato, M. et al. Soft crystals: flexible response systems with high structural order. *Chem. Eur. J.* **25**, 5105–5112 (2019).
15. Lassègues, J. C. et al. Raman and ab initio study of the conformational isomerism in the 1-ethyl-3-methyl-imidazolium bis(trifluoromethanesulfonyl) imide ionic liquid. *J. Raman Spectrosc.* **38**, 551–558 (2007).
16. Kitaura, R. et al. Porous coordination-polymer crystals with gated channels specific for supercritical gases. *Angew. Chem., Int. Ed.* **42**, 428–431 (2003).
17. Aki, S. N. V. K. et al. High-pressure phase behavior of carbon dioxide with imidazolium-based ionic liquids. *J. Phys. Chem. B* **108**, 20355–20365 (2004).
18. Song, H.-J. et al. Simplified estimation of regeneration energy of 30 wt % sodium glycinate solution for carbon dioxide absorption. *Ind. Eng. Chem. Res.* **47**, 9925–9930 (2008).
19. Lu, W. et al. Cost-effective synthesis of amine-tethered porous materials for carbon capture. *ChemSusChem* **8**, 410–410 (2014).

20. Dunne, J. A. et al. Calorimetric heats of adsorption and adsorption isotherms. 1. O_2, N_2, Ar, CO_2, CH_4, C_2H_6, and SF_6 on silicalite. *Langmuir* **12**, 5888–5895 (1996).
21. Dębski, B. et al. Thermodynamic interpretation and prediction of CO_2 solubility in imidazolium ionic liquids based on regular solution theory. *J. Mol. Liq.* **291**, 110477 (2019).
22. Batsanov, S. S. Van der Waals radii of elements. *Inorg. Mater.* **37**, 871–885 (2001).
23. Brigot, N. et al. The structure of the carbon dioxide dimer. *Chem. Phys. Lett.* **49**, 157–159 (1977).
24. Mannik, L. et al. An Infrared spectrum of CO_2 dimers in the "Locked" configuration. *Can. J. Phys.* **49**, 3056–3057 (1971).
25. Bhargava, B. & Balasubramanian, S. Probing anion–carbon dioxide interactions in room temperature ionic liquids: gas phase cluster calculations. *Chem. Phys. Lett.* **44**, 242–246 (2007).
26. Babarao, R. et al. Understanding the high solubility of CO_2 in an Ionic Liquid with the Tetracyanoborate anion. *J. Phys. Chem. B* **115**(32), 9789–9794 (2011).
27. Lourenço, T. C. et al. Local environment structure and dynamics of CO_2 in the 1-ethyl-3-methylimidazolium bis(trifluoromethanesulfonyl)imide and related ionic liquids. *J. Chem. Phys.* **146**, 104502 (2017).
28. Fujii, K. et al. Conformational equilibrium of bis(trifluoromethanesulfonyl) imide anion of a room-temperature ionic liquid: Raman spectroscopic study and DFT calculations. *J. Phys. Chem. B* **110**, 8179–8183 (2006).
29. Hoogerstraete, T. V. et al. Crystal structures of low-melting ionic transition-metal complexes with N-alkylimidazole ligands. *CrystEngComm* **14**, 4902–4911 (2012).
30. Numaguchi, R. et al. Molecular simulation of capillary phase transitions in flexible porous materials. *J. Chem. Phys.* **138**, 054708 (2013).
31. Gurkan, B. et al. Molecular design of high capacity, low viscosity, chemically tunable ionic liquids for CO_2 capture. *J. Phys. Chem. Lett.* **1**, 3494–3499 (2010).
32. Noro, S. et al. Controlling the gate-sorption properties of solid solutions of Werner complexes by varying component ratios. *Dalton Trans.* **49**, 9438–9443 (2020).
33. Henschel, D. et al. Metall(II)-dimethylamid-tetrahydrate: das dimethylamin-anion als einzähniger O-ligand und tetrafunktioneller Wasserstoffbrucken-Akzeptor in den isotypen Komplexen $[M(H_2O)_4\{(CH_3SO_2)_2N\}_2]$ mit M = magnesium, nickel, kupferund zink. *Z. Anorg. Allg. Chem.* **622**, 1065–1075 (1996).
34. Sheldrick, G. M. SHELXT–Integrated space-group and crystal-structure determination. *Acta Cryst.* **A71**, 3–8 (2015).
35. Sheldrick, G. M. Crystal structure refinement with SHELXL. *Acta Cryst.* **C71**, 3–8 (2015).
36. Dolomanov, O. V. et al. OLEX2: a complete structure solution, refinement and analysis program. *J. Appl. Cryst.* **42**, 339–341 (2009).
37. Frisch, M. J. et al. Gaussian 09, Revision E.01 (Gaussian, Inc., Wallingford CT, 2009).
38. Perdew, J. P. et al. Generalized gradient approximation made simple. *Phys. Rev. Lett.* **77**, 3865–3868 (1996).
39. Grimme, S. et al. A consistent and accurate ab initio parametrization of density functional dispersion correction (DFT-D) for the 94 elements H-Pu. *J. Chem. Phys.* **132**, 154104 (2010).
40. Kresse, G. & Hafner, J. Ab initio molecular dynamics for liquid metals. *Phys. Rev. B* **47**, 558–561 (1993).
41. Kresse, G. & Hafner, J. Ab initio molecular-dynamics simulation of the liquid-metal–amorphous-semiconductor transition in germanium. *Phys. Rev. B* **49**, 14251–14269 (1994).
42. Kresse, G. & Furthmüller, J. Efficiency of ab-initio total energy calculations for metals and semiconductors using a plane-wave basis set. *J. Comput. Mat. Sci.* **6**, 15–50 (1996).
43. Kresse, G. & Furthmüller, J. Efficient iterative schemes for ab initio total-energy calculations using a plane-wave basis set. *Phys. Rev. B* **54**, 11169–11186 (1996).
44. Tang, W. et al. A grid-based Bader analysis algorithm without lattice bias. *J. Phys. Condens. Matter.* **21**, 084204 (2009).
45. Sanville, E. Improved grid-based algorithm for Bader charge allocation. *J. Comp. Chem.* **28**, 899–908 (2007).
46. Henkelman, G. A. et al. A fast and robust algorithm for Bader decomposition of charge density. *Comput. Mater. Sci.* **36**, 354–360 (2006).
47. Yu, M. & Trinkle, D. R. Accurate and efficient algorithm for Bader charge integration. *J. Chem. Phys.* **134**, 064111 (2011).
48. Sillar, K. et al. Ab Initio Study of Hydrogen Adsorption in MOF-5. *J. Am. Chem. Soc.* **131**, 4143–4150 (2009).
49. Valenzano, L. et al. Heats of adsorption of CO and CO_2 in metal–organic frameworks: quantum mechanical study of CPO-27-M (M = Mg, Ni, Zn). *J. Phys. Chem. C.* **115**, 21777–21784 (2011).
50. Simpson, S. et al. Modulating bond lengths via backdonation: a first-principles investigation of a quinonoid zwitterion adsorbed to coinage metal surfaces. *J. Phys. Chem. C.* **120**, 6633–6641 (2016).
51. Velde, G. T. et al. Chemistry with ADF. *J. Comput. Chem.* **22**, 931–967 (2001).
52. Lenthe, E. V. et al. Relativistic regular two-component Hamiltonians. *Int J. Quantum Chem.* **57**, 281–293 (1996).
53. Ziegler, T. & Rauk, A. On the calculation of bonding energies by the Hartree Fock Slater method. *Theor. Chim. Acta* **46**, 1–10 (1977).
54. Michalak, A. et al. Bond orbitals from chemical valence theory. *J. Phys. Chem. A* **112**, 1933–1939 (2008).
55. Mitoraj, M. & Michalak, A. Natural orbitals for chemical valence as descriptors of chemical bonding in transition metal complexes. *J. Mol. Model.* **13**, 347–355 (2007).

Acknowledgements

This study was supported financially by a Grant-in-Aid for Scientific Research (No. 18K19864) from MEXT, Japan. One of the authors (X.Z.) was supported by The Ministry of Education, Culture, Sports, Science, and Technology through Program for Leading Graduate Schools (Hokkaido University "Ambitious Leader's Program").

Author contributions

X.Z. and K.F. synthesized and characterized the soft crystals, and measured the absorption isotherms. X.Z. carried out the single-crystal X-ray diffraction analysis for CO_2-loaded crystal. H.S. supported the structural analysis of the CO_2-loaded crystal. K.T. supported the single-crystal X-ray diffraction analysis. Y.H. and J.P. performed the theoretical calculations. All authors contributed to the writing and editing of the manuscript. S.N. and T.N. conceived the project and directed the research.

Competing interests

The authors declare no competing interests.

Additional information

Supplementary information is available for this paper at https://doi.org/10.1038/s42004-020-00390-1.

Correspondence and requests for materials should be addressed to S.-i.N. or T.N.

Reprints and permission information is available at http://www.nature.com/reprints

Publisher's note Springer Nature remains neutral with regard to jurisdictional claims in published maps and institutional affiliations.